Missouri University of Science and Technology

Scholars' Mine

Chemical and Biochemical Engineering Faculty Research & Creative Works

Linda and Bipin Doshi Department of Chemical and Biochemical Engineering

01 Feb 2011

Flow Regime Identification in a Bubble Column Via Nuclear Gauge Densitometry and Chaos Analysis

S. Nedeltchev

A. Shaikh

Muthanna H. Al-Dahhan
Missouri University of Science and Technology, aldahhanm@mst.edu

Follow this and additional works at: https://scholarsmine.mst.edu/che_bioeng_facwork

 Part of the Biochemical and Biomolecular Engineering Commons

Recommended Citation

S. Nedeltchev et al., "Flow Regime Identification in a Bubble Column Via Nuclear Gauge Densitometry and Chaos Analysis," *Chemical Engineering and Technology*, vol. 34, no. 2, pp. 225 - 233, Wiley; Gesellschaft Deutscher Chemiker; Gesellschaft für Chemische Technik und Biotechnologie, Feb 2011.
The definitive version is available at https://doi.org/10.1002/ceat.201000308

This Article - Journal is brought to you for free and open access by Scholars' Mine. It has been accepted for inclusion in Chemical and Biochemical Engineering Faculty Research & Creative Works by an authorized administrator of Scholars' Mine. This work is protected by U. S. Copyright Law. Unauthorized use including reproduction for redistribution requires the permission of the copyright holder. For more information, please contact scholarsmine@mst.edu.

Stoyan Nedeltchev[1,2]
Ashfaq Shaikh[3]
Muthanna Al-Dahhan[2]

[1] Institute of Technical Chemistry, TU Braunschweig, Braunschweig, Germany.

[2] Department of Chemical and Biological Engineering, Missouri University of Science and Technology, Rolla, USA.

[3] Intermediates and Polyester Technology Division, Eastman Chemical Company, Kingsport, USA.

Research Article

Flow Regime Identification in a Bubble Column via Nuclear Gauge Densitometry and Chaos Analysis*

The bubble column performance can change significantly as a result of flow regime change. Since reactor volume productivity, mass and heat transfer as well as mixing are affected by the prevailing flow regime, it is very important to know how to identify it. In this work, flow regime identification was performed on the basis of the Kolmogorov entropy (KE) algorithm applied to nuclear gauge densitometry data. In addition, the average cycle time was used for validation of the results. Three transition velocities were identified that delineated the boundaries of the three main hydrodynamic regimes. The first two transition points were also confirmed by the information entropy concept. The increasing KE trend in the bubbly flow regime and the decreasing KE trend in the churn-turbulent regime were predicted successfully by means of new semi-theoretical models.

* *Presented as a poster (Contribution No. 319) at the 21st International Symposium on Chemical Reaction Engineering (ISCRE 21), June 13–16, 2010, Philadelphia (PA), USA.*

Keywords: Bubble columns, Chaotic behavior, Information entropy, Kolmogorov entropy modeling, Nuclear gauge densitometry

Received: July 19, 2010; *revised:* November 03, 2010; *accepted:* November 16, 2010

DOI: 10.1002/ceat.201000308

1 Introduction

Bubble columns are one of the most important gas-liquid contactors. The two- and three-phase cocurrent bubble columns are being used for a wide variety of processes: Fischer-Tropsch, hydrocracking, coal liquefaction, fermentation, hydrogenation, etc. Many of these processes operate at high temperature and pressure, and they are characterized by more complicated hydrodynamics. A thorough understanding of the flow structure in bubble columns is crucial for both their design and scale-up. The flow structure in gas-liquid systems is complicated not only with regard to the micro-scale behavior of single bubbles, such as bubble shape, bubble oscillation, bubble wake and path instability, but also with regard to macro-scale phenomena of the entire gas-liquid dispersion. Liquid movement and bubble properties, e.g., liquid circulation, bubble size distribution and two-phase structures, as well as the mode of gas-liquid interaction are quite different depending on various flow regimes.

Each flow regime transition is usually influenced by many factors, such as column geometry, sparger design, and operating conditions. The study of flow transition is important for improvement of design, operation, and control of the reactor. The bubble column performance can change significantly as a result of flow regime change. Since reactor volume productivity, heat and mass transfer as well as mixing are affected by the prevailing flow regime, it is very important to know how to identify it. However, the determination of flow transition and flow regime boundaries is not easy due to complicated mechanisms. Both the interfacial area and the transport coefficients in a bubble column are highly dependent on the prevailing operating regime, and thus the prediction of the regime transition point is of primary importance. Reliable methods for regime transition identification can be used for design purposes.

A vast number of both experimental and simulation studies on bubble column reactors can be found in the literature. These reactors are characterized by high heat and mass transfer rates, absence of moving parts, large interfacial areas, low operating and maintenance costs, little floor space requirements, and the possibility of operation with solids without serious erosion or plugging problems. Despite their simple construction and operation, bubble columns can be rather difficult to design and scale-up in view of their highly complicated hydrodynamics.

The bubble column can operate under three different hydrodynamic regimes (homogeneous, transition, and heteroge-

Correspondence: Dr. S. Nedeltchev (snn13@gmx.net), Institute of Technical Chemistry, TU Braunschweig, Hans-Sommer-Straße 10, 38106 Braunschweig, Germany

 © 2011 WILEY-VCH Verlag GmbH & Co. KGaA, Weinheim

neous). At low superficial gas velocities u_G, the homogeneous (bubbly flow) regime occurs, in which the dispersion consists of bubbles that are roughly uniform in size. At high u_G values (beyond the transitional gas velocity), the heterogeneous (churn-turbulent) regime occurs. In this flow regime there is a wide bubble size distribution depending on the system properties [1]. At high u_G values, a wide gas phase residence time distribution is usually observed, which is often detrimental to reactor conversion and selectivity.

In the homogeneous flow regime, small, uniform-sized bubbles are observed, whose ascension trajectories are practically vertical or exhibit small-scale transverse and axial oscillations. There is little interaction between individual bubbles, and the breakage and coalescence frequencies are low. At high gas velocities, coalescence and breakage phenomena become more pronounced, leading to a wide variety of bubble sizes, which characterizes the heterogeneous regime. In this flow regime, the bubble trajectories are completely irregular, an almost parabolic gas holdup profile develops, and intense liquid circulation is observed. The change from the homogeneous to the heterogeneous regime occurs gradually, through the so-called transition regime. In the case of most industrial facilities, operation at the heterogeneous regime is desired, but for some bioreactors the homogeneous regime is preferred. It is worth noting that the bed aspect ratio affects the regime transition velocities only when it is smaller than 5 [2–5]. Giovannettone et al. [6] discussed the existence of bubbly flow, slug flow, and annular flow. They mentioned that the bubbly flow is stable at u_G values up to 0.05–0.08 m s^{-1}.

The regime transition point occurs mainly as a result of increasing coalescence. The flow pattern is dictated by the processes of bubble coalescence and breakage. Reilly et al. [1] found that the transition gas velocity from the bubbly flow to the churn-turbulent flow regime depends on the gas density. Liquid properties also affect the transition point. Grover et al. [2] reported that the gas velocity for transition from bubbly flow to churn-turbulent flow decreases with increasing temperature. According to the authors, this is caused by the increased coalescence. The mechanism of bubble coalescence at higher temperatures is not clearly understood. Grover et al. [2] concluded that the increase in temperature has a considerable effect on the flow regime characteristics in bubble columns.

There are several approximate flow regime maps [3, 7] in the literature, but none of them covers a wide range of industrial conditions. Semi-theoretical transition criteria have been developed by Shnip et al. [8], Ruzicka and Thomas [9], and Thorat and Joshi [10]. Ribeiro [11] proposed new empirical formulas for estimating the gas superficial velocity at the point of regime transition in bubble columns and the corresponding gas holdup. Earlier, Kelkar [12] developed a correlation for the transition velocity based on the concept of slip velocity. Reilly et al. [1], Wilkinson and coworkers [13], and Sarrafi et al. [14] also developed correlations for estimation of the transitional gas holdup and gas velocity. Kazakis et al. [4] proposed a correlation for the transitional gas velocity in the case of bubble columns operating with porous plate spargers. Vial et al. [5] and Shaikh and Al-Dahhan [15] summarized the various methods for identifying the regime transition point in bubble columns. For this purpose, most frequently the gas holdup values are used or the dynamic fluctuations of a signal related to the flow pattern (usually wall pressure).

1.1 Various Flow Regimes

Knowledge of flow regimes is most essential in bubble column design. One of the most frequent problems in chemical reactor design involves flow regime identification. Each flow regime transition is strongly dependent on the physicochemical properties of the fluid phases, besides the reactor dimensions and the type of gas distributor.

A reasonable amount of data is available on flow regimes and their transitions in the field of bubble columns. The way in which the gas bubbles are being formed is more complex than is generally supposed, and that is why the description and classification of the various flow regimes is a very important research goal. McCann and Prince [16] identified static, dynamic, and turbulent regimes of bubbling. The static regime occurs only at very low gas flow rates, whereas the turbulent regime occurs at high gas flow rates. In this regime, the bubbles coalesce close to the orifice, and the two merged bubbles rise only a small distance (about 0.1 m) above the orifice before they are shattered into many small bubbles of varying sizes. At still higher gas flow rates, irregular bubbles rise in a rapid swirling motion and inertial forces become quite pronounced. The authors argue that the transition between regimes is not sharp. It depends on the liquid physical properties, orifice size, chamber volume, and the gas flow rate.

At low u_G values (bubbly flow regime), the gas holdup is nearly directly proportional to the gas velocity (exponent: 0.7–1.2). Then a point is reached where a rather abrupt change occurs. At gas velocities u_G above this point (i.e. in the churn-turbulent regime), the gas holdup continues to increase with u_G, but the rate of change is significantly lower (exponent: 0.4–0.7). Reilly et al. [1] reported that, in the bubbly flow regime, the gas holdup is directly proportional to the specific gas phase momentum, whereas in the churn-turbulent regime the gas holdup is proportional to the cube root of momentum.

Ruzicka et al. [17] and Nedeltchev et al. [18, 19] well described the three major flow regimes in bubble columns. The homogeneous (dispersed bubble) regime is characterized by relatively small uniform bubbles (narrow bubble size distribution) which cause gentle agitation of the gas-liquid dispersion. The gas sparger plays an important role. Bubble coalescence is insignificant. A relatively uniform gas holdup profile and a flat liquid velocity profile are observed. The transition from the bubbly flow regime to the churn-turbulent regime is a gradual process.

Large flow macrostructures (large eddies) and local liquid circulation patterns are being formed in the transition regime. The bubble coalescence becomes significant. This flow regime is characterized by a widened bubble size distribution. The boundaries of the transition regime depend on the quality of aeration. Recently, Olmos et al. [20, 21] and Barghi et al. [22] provided evidence of the existence of both first and second transition regimes. In the first sub-regime, bubble coalescence can be seen only in the sparger region, whereas in the second

 © 2011 WILEY-VCH Verlag GmbH & Co. KGaA, Weinheim

15214125, 2011, 2, Downloaded from https://onlinelibrary.wiley.com/doi/10.1002/ceat.201000308 by Missouri University Of Science, Wiley Online Library on [10/04/2023]. See the Terms and Conditions (https://onlinelibrary.wiley.com/terms-and-conditions) on Wiley Online Library for rules of use; OA articles are governed by the applicable Creative Commons License

sub-regime bubble coalescence and breakup (along with gross liquid circulation) occur in all zones of the reactor. In the second transition regime a global liquid flow macrostructure appears.

As u_G increases further, larger bubbles begin to form, whose wakes cause gross circulation patterns leading to the establishment of the churn-turbulent (coalesced bubble) regime. The latter is characterized by a large bubble size distribution and a radial gas holdup profile that causes large-scale liquid circulation. Bubbles coalesce in the vicinity of the gas sparger to create large bubbles. The churn-turbulent flow regime is characterized by vigorous mixing. Deckwer [7] argues that in this flow regime the gas sparger has little effect. Fan and coworkers [23, 24] reported the existence of four sub-regimes in the churn-turbulent regime. Comprehension of the mechanisms of regime transition is of crucial importance for modeling, design, and optimization of bubble columns. The underlying mechanism for regime transition is not yet clearly revealed and there is still no general consensus on its explanation.

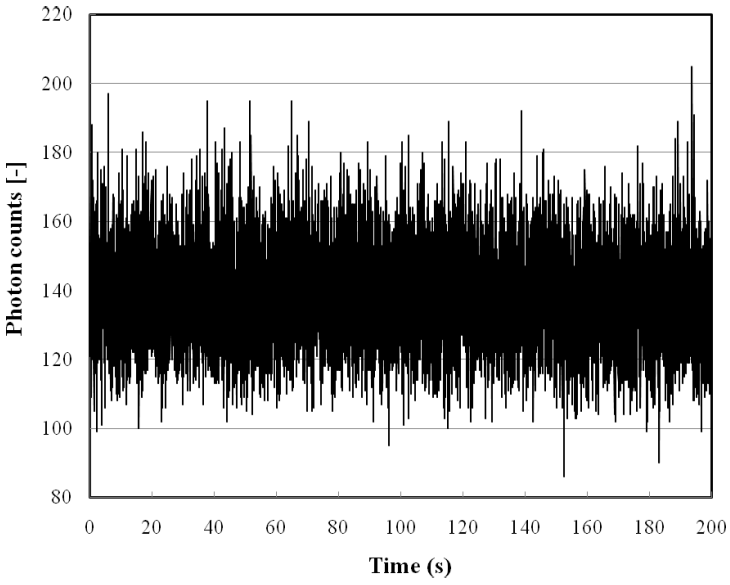

Figure 1. Time series of photon counts in a bubble column operated with an air-water system at $u_G = 0.03\ m\ s^{-1}$ and ambient conditions.

1.2 Kolmogorov Entropy Algorithm

The Kolmogorov entropy (KE) is a sensitive and robust invariant for the dynamics of bubble columns and can be used to determine differences in dynamic behavior for varying operating conditions, to quantitatively assess the dynamic similarity between scaled bubble columns and to characterize and classify different hydrodynamic regimes. In general, KE is large for very irregular dynamic behavior (such as pressure fluctuations in turbulent bubble columns), while it is small in the case of a more regular behavior. There are basically two algorithms for KE calculation [25, 26]. The method of Schouten et al. [26] has gained more popularity due to its successful application for flow regime classification based on time series analysis of pressure fluctuations in both gas-solid fluidized beds and bubble columns. In this method, the KE is calculated from the average number of steps required for a pair of vectors X_i and X_j, which are initially within a specific maximum length l_0, to separate until the distance between the pair becomes larger than l_0. Generally speaking, the points in an experimental time series are measured at discrete, constant time intervals with a time step between two sampled data points that equals $1/f_s$, where f_s is the sampling frequency. The maximum-likelihood estimator of the KE [26] can be expressed as follows:

$$KE = -f_s \ln\left(1 - \frac{1}{\bar{b}}\right) \tag{1}$$

$$\bar{b} = \frac{1}{M}\sum_{i=1}^{M} b_i \tag{1a}$$

The variable b equals the number of sequential pairs of points on the attractor, given an initial pair of independent points X_i and X_j within a distance l_0, in which the interpoint distance l is for the first time bigger than the specified maximum interpoint distance l_0. The above-described KE algorithm [26] was applied to various time series of photon counts that looked similar to the ones depicted in Fig. 1.

In the present analysis, the distance between two reconstructed state vectors X_i and X_j was estimated on the basis of the maximum norm definition [26]. For all the pairs of points on the attractor, the number of steps is calculated and then the average number is estimated. This can be done by counting the number of steps in time that the (initial) distance between the points can be followed along the attractor before it becomes larger than some prescribed distance (the so-called *cut-off* distance l_0). A good practical description of the KE algorithm (including some examples) is available from Van den Bleek and Schouten [27].

In most of the cases, the number of vector elements (embedding dimension) is set equal to 50 [18, 19, 28] and the delay time is chosen to be unity. The cut-off length can be fixed at one, two or three times the average absolute deviation (AAD) (which is a robust estimator of the data width around the average value). The number of elements, m, of the state vector is equal to the number of coordinates in the reconstructed state space. In the literature, often the researchers refer to m as an embedding dimension and it provides the number of degrees of freedom [27]. In this work, an embedding dimension of 50, a delay time of 1, and a cut-off length equal to 3 AAD were used.

2 Nuclear Gauge Densitometry

A nuclear gauge densitometer is made up of a sealed source in a holder and a scintillation detector in front of the source. The source holder and the detector are mounted at the opposite ends of the column. A focused beam of radiation is transmitted from the source, through the column and process material, to the detector. The amount of radiation reaching

 © 2011 WILEY-VCH Verlag GmbH & Co. KGaA, Weinheim

15214125, 2011, 2, Downloaded from https://onlinelibrary.wiley.com/doi/10.1002/ceat.201000308 by Missouri University Of Science, Wiley Online Library on [10/04/2023]. See the Terms and Conditions (https://onlinelibrary.wiley.com/terms-and-conditions) on Wiley Online Library for rules of use; OA articles are governed by the applicable Creative Commons License

the detector from the source depends on the density of the material in the column. It is generally believed that the amount of radiation that reaches the detector through the process material is reflective of its flow behavior and properties. Typical time series of photon counts are presented in Fig. 1.

Nuclear gauge densitometry (NGD) is used extensively in the industry for such applications as level monitoring and control, density measurement, interface identification, and weight measurements in conveyors. Recently, Shaikh and Al-Dahhan [29, 30] have developed a new method for online flow regime monitoring in bubble columns based on NGD. This technique is characterized by robustness and it is widely used in the following industries: chemicals, petrochemicals, offshore oil and gas, pharmaceuticals, cement, quarrying, solids handling, paper and food. NGD is an *active* technique, i.e. it involves penetration of gamma-rays through the column and therefore it should reliably represent the hydrodynamics (even under industrial conditions). NGD appears to be a more robust technique than gamma-ray computed tomography, both on the laboratory and the industrial scale. A particularly important advantage is the fact that NGD can be implemented without disturbing the operation of the reactor.

The major advantages of NGD that make it attractive in everyday industrial use are as follows:

- Non-intrusive: Since the sources and detectors are mounted externally from the column, they are completely unaffected by the conditions inside, providing reliable solutions when other technologies fail. They can be easily accessed, installed or removed, without affecting or interrupting the process.
- High integrity: A non-invasive system mounted outside the column means no exposure or wear by corrosive or abrasive products, and no need for construction to resist high-pressure, high-temperature process conditions. This means less risk of leaks or emissions, protecting processes, people, and the environment.
- High reliability and low maintenance: NGD measurements offer reliability and long-term performance. In addition, source checking is routine, simple and can be planned well in advance.
- Low installation costs: NGD can often be installed and commissioned without process shutdown. Also, in most applications, no alterations to the reactors/columns are needed, which means no expensive design changes for such implementation of NGD.

3 Experimental

Nonintrusive NGD measurements were performed in the middle of a plexiglass bubble column (0.1 m in ID, 1.2 m in height) operated with an air-water system at ambient conditions. They were used for gas holdup estimation and also for flow regime identification.

The gamma-ray source (Cs-137, 100 mCi) and the detector were mounted on a plate that can move in axial direction. The detector consists of a cylindrical 0.051×0.051 m NaI crystal, a photo-multiplicator (PM), and electronics, forming a 0.054×0.26 m cylindrical assembly. The collimator ($1.59 \cdot 10^{-3} \times 4.8 \cdot 10^{-3}$) was placed in front of the detector. The photon count rate (which was converted from the output voltage) was recorded by means of an automated data acquisition system. A multichannel analyzer was used to measure the energy spectrum of the gamma photons. During the experiments, a focused beam of radiation was transmitted from the source (Cs-137) through the column and process material to the scintillation detector (Fig. 2). The photon count history was collected at a sampling frequency of 50 Hz for an acquisition time period of 300 s. NGD measures the spatial variation of the attenuation coefficient of gamma photons, which is linearly related to the gas holdup distribution. The details of the experimental setup and the technique can be found elsewhere [29, 30].

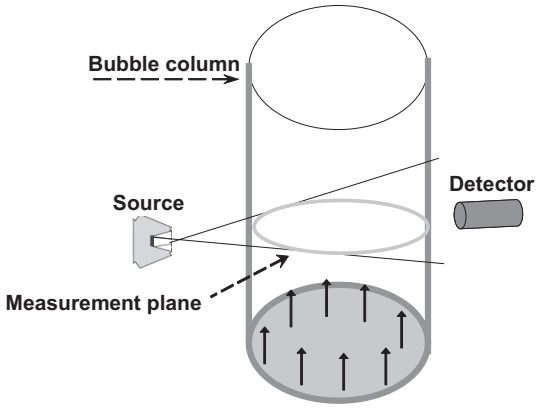

Figure 2. Gamma-ray densitometry setup.

The superficial gas velocities u_G were varied from 0.01 up to 0.11 m s^{-1} with a step of 0.005 m s^{-1} around the first transition velocity. The bubble column was equipped with a gas sparger consisting of 64 holes of $1.32 \cdot 10^{-3}$ m in ID with an open area of 1.09 %.

The NGD scans were repeated three times and then averaged. The mean relative error was less than 3 %. The photon count history (of length 10 000 points) was treated by means of the KE algorithm [26], which is a part of the nonlinear chaos theory. The number of vector elements (embedding dimension) was set equal to 50, the delay time was chosen to be unity, and the cut-off length was fixed at three times the AAD (which is a robust estimator of the data width around the average value). At each operating condition, three measurements were run and the average value was taken. The data reproducibility was acceptable (within ±5 %).

4 Results and Discussion

Fig. 3 shows the KE values derived from NGD data as a function of the superficial gas velocity u_G. The error in the calculation of each local KE value was always less than 5 %. Three KE peaks (points of instability) are distinguishable, which correspond to three transitional gas velocities. At $u_G = 0.035$ m s^{-1}, the first transitional gas velocity occurs. At this point the bubbly flow regime transforms itself into the first transition regime. It is worth noting that, in the case of an air-water system aerated (under ambient conditions) in a similar bubble

 © 2011 WILEY-VCH Verlag GmbH & Co. KGaA, Weinheim

15214125, 2011, 2, Downloaded from https://onlinelibrary.wiley.com/doi/10.1002/ceat.201000308 by Missouri University Of Science, Wiley Online Library on [10/04/2023]. See the Terms and Conditions (https://onlinelibrary.wiley.com/terms-and-conditions) on Wiley Online Library for rules of use; OA articles are governed by the applicable Creative Commons License

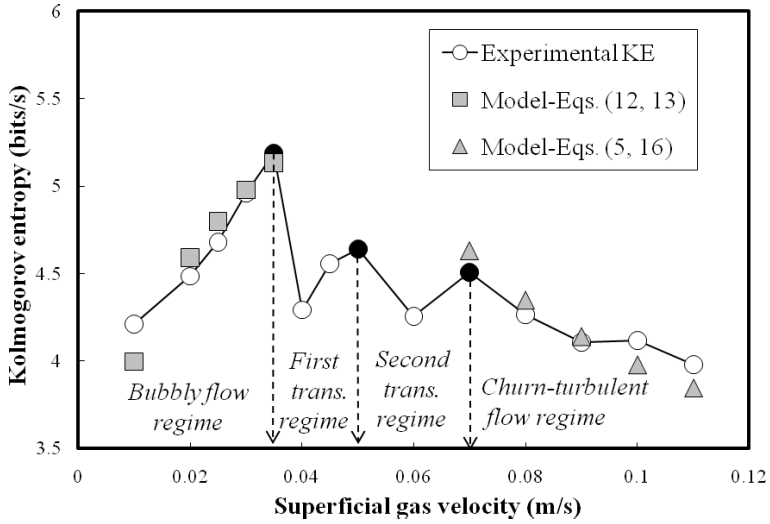

Figure 3. Kolmogorov entropy (KE) profile as a function of the superficial gas velocity u_G in a bubble column operated with an air-water system under ambient conditions.

column (0.1 m in ID), Grover et al. [2] reported that the first transition occurs at 0.031 m s^{-1}. The authors used only a different gas distributor (sintered glass disc, mean pore size: 100–120 μm).

At $u_G = 0.05$ m s^{-1} follows another transition between two sub-regimes: the first and second transition regimes. Jamialahmadi and Müller-Steinhagen [31] reported that the transition from the bubbly flow regime to the transition regime occurs at 0.04 m s^{-1}, and the one from the transition regime to the churn-turbulent regime occurs at 0.06 m/s. Lin et al. [32] reported that the real transition regime starts at 0.049 m s^{-1}.

Finally, at $u_G = 0.07$ m s^{-1}, the onset of the fully developed churn-turbulent regime is observed. In this flow regime, the gamma-rays are frequently intercepted by bubbles of different sizes and intensity, giving rise to higher fluctuations. Fig. 3 exhibits also that there are two KE minima, which could be interpreted as points of stability.

The three transition velocities can be predicted theoretically. In order to calculate the first transitional gas velocity U_{trans}, the correlation for the transitional gas holdup [1] should be used:

$$\varepsilon_{trans} = 0.5\, B^{1.5} \sqrt{\frac{\rho_G^{0.96}\sigma^{0.12}}{\rho_L}} \qquad (2)$$

The authors reported that $B = 4.3$. The substitution of this value into Eq. (2) yields $\varepsilon_{trans} = 0.129$ (air-water system). It is noteworthy that Krishna et al. [33] reported practically the same transitional gas holdup (0.12) for an air-water system aerated in a smaller bubble column (0.05 m in ID) equipped with a sintered glass plate (20–40 μm). The experimental gas holdup values are presented in Fig. 4. By means of interpolation, it can be found that the value 0.129 corresponds to $u_G = 0.033$ m s^{-1}, which should be considered as a theoretical transition velocity U_{trans}.

It is reasonable to assume that, at the second U_{trans} value, both small and large bubbles coexist. First, the focus is on the estimation of the large bubble diameter d_b^*. It has been found that, at the second U_{trans} value, the bubble shape (and thus the flow pattern) changes from oblate to prolate ellipsoidal. This fact is also supported by the bubble shape diagrams of Clift et al. [34] and Fan and Tsuchiya [35]. According to Terasaka et al. [36], this transition occurs at Ta = 6, where

$$\mathrm{Ta} = \mathrm{Re_b Mo}^{0.23} = \left(\frac{U_b d_b^* \rho_L}{\mu_L}\right)\left(\frac{g\,\mu_L^4}{\rho_L \sigma^3}\right)^{0.23} \qquad (3)$$

When the formula for the rise velocity of large bubbles [37]

$$U_b = 1.95 D_c^{0.167}\left(g d_b^*\right)^{0.5} = 4.158\, d_b^{*\,0.5} \qquad (4)$$

is substituted into Eq. (3), one can calculate that at the second transitional velocity (Ta = 6) the large bubble size d_b^* is $5.4\cdot10^{-3}$ m. Nedeltchev [38] simplified the model equation for large bubble sizes developed by Darton et al. [39] based on the bubble coalescence model and derived the following equation:

$$d_b^* = 0.659\,(u_G - U_{trans})^{1.2} \qquad (5)$$

It is worth noting that Eq. (5) was first used in the field of bubble columns by Ellenberger and Krishna [37] and Krishna et al. [40] on the basis of the hydrodynamic analogies between fluidized beds and bubble columns.

When we substitute $d_b^* = 5.4\cdot10^{-3}$ m and $U_{trans} = 0.033$ m s^{-1} into Eq. (5), we obtain that the second critical u_G value is equal to 0.051 m s^{-1}. Fig. 3 shows that the second KE peak occurs at $u_G = 0.05$ m s^{-1}; this value practically coincides with the theoretical prediction. The transitional gas holdup at this u_G value is 0.205 (Fig. 4).

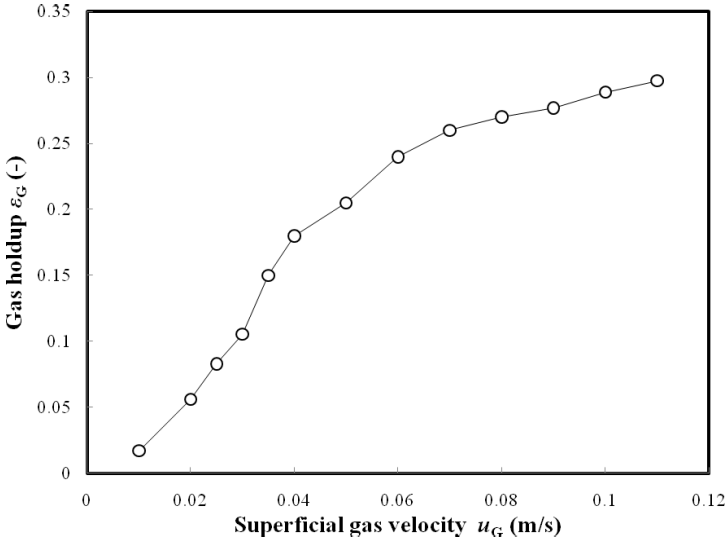

Figure 4. Gas holdup profile as a function of the superficial gas velocity u_G in a bubble column operated with an air-water system under ambient conditions.

© 2011 WILEY-VCH Verlag GmbH & Co. KGaA, Weinheim

15214125, 2011, 2, Downloaded from https://onlinelibrary.wiley.com/doi/10.1002/ceat.201000308 by Missouri University Of Science, Wiley Online Library on [10/04/2023]. See the Terms and Conditions (https://onlinelibrary.wiley.com/terms-and-conditions) on Wiley Online Library for rules of use; OA articles are governed by the applicable Creative Commons License

According to Terasaka et al. [36], at a Tadaki number Ta equal to 16.5, the bubble shape changes again from prolate ellipsoidal to spherical cap. This causes a change of the flow pattern and can be identified as a third regime transition. When we substitute Ta = 16.5 into Eq. (3) and take into account Eq. (4), we obtain $d_b^* = 10.5 \cdot 10^{-3}$ m. The substitution of this d_b^* value along with $U_{trans} = 0.033\ m\ s^{-1}$ into Eq. (5) yields $u_G = 0.065\ m\ s^{-1}$. Fig. 3 shows that the third KE peak occurs at $u_G = 0.07\ m\ s^{-1}$. The difference between both values is acceptable. It should be mentioned that, if the real first transition velocity of $0.035\ m\ s^{-1}$ is used, the theoretical value ($0.067\ m\ s^{-1}$) becomes closer to the experimental value ($0.07\ m\ s^{-1}$). Jamialahmadi and Müller-Steinhagen [31] reported a transitional velocity of $0.06\ m\ s^{-1}$. Fig. 4 shows that the third transitional gas holdup is 0.26.

The average cycle time T_c can also be used as an indicator of flow regime transitions. Fig. 5 shows that two transition velocities U_{trans} (0.035 and $0.07\ m\ s^{-1}$) can be successfully identified. It is worth noting that these U_{trans} values coincide with the first and third transition velocities identified on the basis of the KE values (Fig. 3). At both superficial gas velocities, the average cycle time T_c exhibits well pronounced changes in its rate of increase. The error in the calculation of each local T_c value was always less than 5 %.

4.1 Identification of the Main Transition Velocities Based on Information Entropy

The information entropy (IE) algorithm well described by Nedeltchev et al. [41–44] was also used to independently identify the main regime transition velocities. At first, the minimum and maximum values in each signal were determined. Then, the range was divided into different regions (cylindrical shells (volumes)) with progressively increasing height (10, 20, 30, 40 and 50). Since their diameter was kept constant, it was practically eliminated. The volume of the smallest region (with a height of 10) was used as the unit volume V_0. Following Nedeltchev et al. [41–44], the probability of a signal visiting a certain range of values ($V_1, V_2, V_3, ...$) can be expressed as follows:

$$P_i = \frac{V_0}{V_i} \frac{N_v V_i}{\sum_{i=1}^{N} N_v V_i} \quad (6)$$

The information amount is a function of the probability P_i:

$$I_i = -\log(P_i) \quad (7)$$

The total information entropy H is a function of both parameters:

$$H = \sum_{i=1}^{N} \frac{V_i}{V_0} P_i I_i \quad (8)$$

Fig. 6 shows the IE profile as a function of the superficial gas velocity u_G. Two of the transition velocities (at 0.03 and $0.05\ m\ s^{-1}$) as identified by the KE algorithm are clearly identifiable by the IE values as well. At these points, sudden changes of the IE profile are observed. The error in the calculation of each local IE value was always less than 5 %.

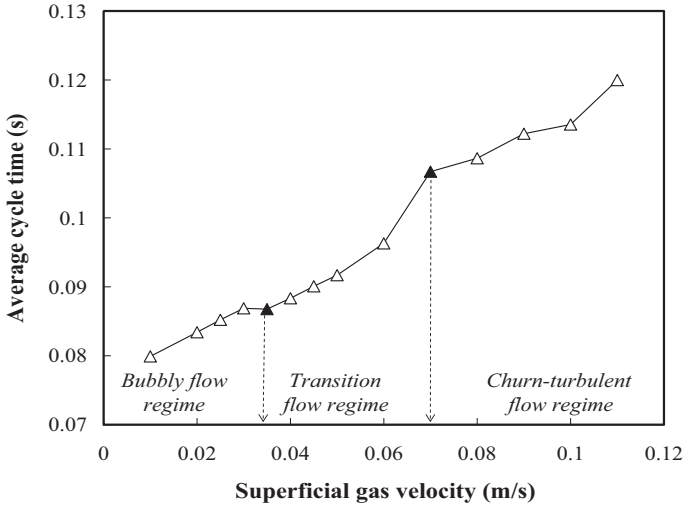

Figure 5. Profile of the average cycle time as a function of the superficial gas velocity u_G in a bubble column operated with an air-water system under ambient conditions.

Between 0.03 and $0.05\ m\ s^{-1}$ the IE values increase slightly, whereas above $0.05\ m\ s^{-1}$ a well-pronounced increase is observed. So, the results from the KE approach are confirmed additionally by the IE algorithm. It is worth noting that this algorithm implies also that, at 0.02 m/s, the flow pattern changes (transition from chain-bubbling to bubbly flow regime). This explains why the KE model in the bubbly flow regime is not well capable of predicting the KE value at $0.01\ m\ s^{-1}$. The IE algorithm is very simple and it is applied for the first time to NGD data.

4.2 Prediction of the KE Values in the Bubbly Flow Regime

The KE values can be theoretically predicted by correlating them to both bubble formation frequency and bubble impact [43]:

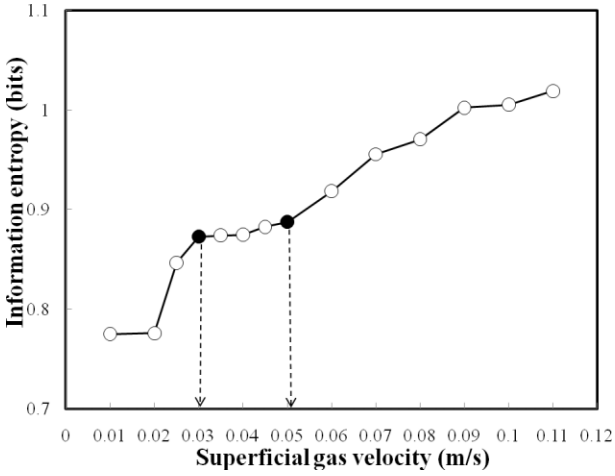

Figure 6. Profile of the information entropy as a function of the superficial gas velocity u_G in a bubble column operated with an air-water system under ambient conditions.

 © 2011 WILEY-VCH Verlag GmbH & Co. KGaA, Weinheim

15214125, 2011, 2, Downloaded from https://onlinelibrary.wiley.com/doi/10.1002/ceat.201000308 by Missouri University Of Science, Wiley Online Library on [10/04/2023]. See the Terms and Conditions (https://onlinelibrary.wiley.com/terms-and-conditions) on Wiley Online Library for rules of use; OA articles are governed by the applicable Creative Commons License

$$\text{KE} = C\ (\text{bubble formation frequency})\ (\text{bubble impact}) \quad (9)$$

where C is a proportionality constant.

Following Nedeltchev et al. [43], the bubble formation frequency can be expressed as follows:

$$\text{bubble formation frequency} = \frac{Q_G}{V_b} = \frac{u_G \pi D_c^2}{4N_h \frac{\pi d_b^3}{6}} = \frac{1.5\ u_G D_c^2}{N_h d_b^3} \quad (10)$$

On the other hand, the bubble impact can be estimated as:

$$\text{bubble impact} = \frac{d_b}{D_c} \quad (11)$$

The substitution of Eqs. (10) and (11) into the model equation (9) yields:

$$\text{KE} = 1.5\ C\ \frac{u_G D_c}{N_h d_b^2} \quad (12)$$

The bubble size d_b can be predicted by means of the correlation of Miller [45]:

$$d_b = 1.492 \left(\frac{u_G D_c^2}{4N_h}\right)^{0.4} \quad (13)$$

According to Eq. (13), the bubble sizes d_b vary in the range of $5.36 \cdot 10^{-3}$–$5.7 \cdot 10^{-3}$ m for $0.01 \le u_G \le 0.035\ \text{m s}^{-1}$ (bubbly flow regime). By means of nonlinear regression analysis, it was determined that $C = 2.834$. All five KE values in the bubbly flow regime were fitted with an average relative error of 2.3 %. The maximum relative error (at $u_G = 0.01\ \text{m s}^{-1}$) is 5.1 %.

4.3 Prediction of the KE Values in the Churn-Turbulent Flow Regime

The churn-turbulent regime is characterized by the existence of large (spherical-cap) bubbles that are rising in the core of the bubble bed. The model equation (10) can be applied to the churn-turbulent regime in case that the large-bubble formation frequency is considered. In other words, Eq. (10) should be modified as follows:

$$\text{large bubble formation frequency} = \frac{1.5\ (u_G - U_{trans})\ D_c^2}{N_h d_b^{*3}} \quad (14)$$

The large bubble impact in the churn-turbulent regime should play a more important role and it can be expressed as follows:

$$\text{large bubble impact} = \left(\frac{d_b^*}{D_c}\right)^2 \quad (15)$$

The substitution of Eqs. (14) and (15) into Eq. (9) yields:

$$\text{KE} = 1.5\ \text{C}\ \frac{(u_G - U_{trans})}{N_h d_b^*} \quad (16)$$

The diameter of the large, spherical-cap bubbles can be estimated by using Eq. (5) based on the simplified bubble coalescence model. The derivation of this equation can be found in [38]. The theoretically predicted value $0.033\ \text{m s}^{-1}$ should be used as the transitional gas velocity U_{trans} (at which the first large bubble forms). The large bubble sizes d_b^* vary in the range of $12.8 \cdot 10^{-3}$–$30.6 \cdot 10^{-3}$ m for the u_G values (0.07–0.11 m s^{-1}) tested in the churn-turbulent regime. By means of nonlinear regression analysis, it was determined that $C = 66.015$. All five KE values in the churn-turbulent regime were fitted with an average relative error of 1.4 %. The maximum relative error (at $u_G = 0.1\ \text{m s}^{-1}$) is 2.1 %.

5 Conclusion

In this work, it was demonstrated how the nonlinear chaos theory could be applied successfully to NGD data for the sake of flow regime identification. The boundaries of bubbly flow, for both the first and second transition regimes as well as the churn-turbulent regime, were delineated and compared with appropriately selected theoretical predictions. By means of the KE algorithm, three transitional gas velocities U_{trans} (0.035, 0.05 and 0.07 m s^{-1}) were identified, respectively. The first and the third U_{trans} values were additionally verified by calculating the average cycle time and plotting it versus the superficial gas velocity. On the other hand, by means of the IE algorithm, the first and second U_{trans} values were verified.

In both the bubbly and churn-turbulent flow regimes, the KE was correlated successfully to bubble formation frequency and bubble impact. In the bubbly flow regime, the initially formed bubbles were considered, whereas in the fully developed churn-turbulent regime only the large spherical-cap bubbles were taken into account. Due to the existence of large bubbles in the churn-turbulent regime, it was assumed that their bubble impact is much stronger. The developed KE correlations can be used for scale-up purposes by keeping the (dimensionless) KE in two reactors constant, in order to realize identical mass and heat transfer as well as mixing.

Acknowledgement

S. Nedeltchev acknowledges the financial support of the European Commission (7th Framework Programme, Marie Curie Outgoing International Fellowship, Grant Agreement No. 221832) for his participation in this research. A. Shaikh and M. Al-Dahhan are grateful for the High Pressure Slurry Bubble Column Reactor (HPSBCR) Consortium (ConocoPhillips (USA), EniTech (Italy), Sasol (South Africa), Statoil (Norway)) and UCR-DOE (DE-FG-26-99FT40594) grants that made this work possible.

The authors have declared no conflict of interest.

Symbols used

b	[–]	number of sequential pair of points on the attractor when $l < l_0$
B	[–]	constant in Eq. (2)
C	[–]	constant of proportionality in Eq. (9)

 © 2011 WILEY-VCH Verlag GmbH & Co. KGaA, Weinheim

15214125, 2011, 2, Downloaded from https://onlinelibrary.wiley.com/doi/10.1002/ceat.201000308 by Missouri University Of Science, Wiley Online Library on [10/04/2023]. See the Terms and Conditions (https://onlinelibrary.wiley.com/terms-and-conditions) on Wiley Online Library for rules of use; OA articles are governed by the applicable Creative Commons License

d_b	[m]	bubble diameter in the bubbly flow regime
d_b^*	[m]	large ("equilibrium") bubble diameter
D_c	[m]	column diameter
f_s	[s^{-1}]	sampling frequency
g	[m s^{-2}]	acceleration due to gravity
H	[bits]	information entropy
I	[–]	information amount
KE	[bits s^{-1}]	Kolmogorov entropy
l	[–]	interpoint distance
l_0	[–]	maximum interpoint distance
M	[–]	sample size of b values
Mo	[–]	Morton number, Eq. (1)
m	[–]	embedding dimension
N	[–]	number of regions visited by the signal
N_v	[–]	number of visits in each region
N_h	[–]	number of distributor holes
P	[–]	probability of a signal visiting a certain range of values
Q_G	[$m^3 s^{-1}$]	gas flow rate
Re_b	[–]	bubble Reynolds number, Eq. (1)
Ta	[–]	Tadaki number, Eq. (1)
T_c	[s]	average cycle time
U_b	[m s^{-1}]	large bubble rise velocity, Eq. (4)
u_G	[m s^{-1}]	superficial gas velocity
U_{trans}	[m s^{-1}]	transitional gas velocity
V	[m^3]	volume of the region visited by the signal
V_0	[m^3]	unit volume
V_b	[m^3]	bubble volume
X	[–]	state vector

Greek symbols

ε_{trans}	[–]	transitional gas holdup
μ_L	[Pa s]	liquid viscosity
ρ_G	[kg m^{-3}]	gas density
ρ_L	[kg m^{-3}]	liquid density
σ	[N m^{-1}]	surface tension

Subscript

i	number of region visited by the signal

References

[1] I. G. Reilly, D. S. Scott, T. J. W. Bruijn, D. MacIntyre, *Can. J. Chem. Eng.* **1994**, *72*, 3.

[2] G. S. Grover, C. V. Rode, R. V. Chaudhari, *Can. J. Chem. Eng.* **1986**, *64*, 501.

[3] Y. T. Shah, B. G. Kelkar, S. P. Godbole, W.-D. Deckwer, *AIChE J.* **1982**, *28*, 353.

[4] N. A. Kazakis, I. D. Papadopoulos, A. A. Mouza, *Chem. Eng. Sci.* **2007**, *62*, 3092. DOI: 10.1016/j.ces.2007.03.004

[5] C. Vial, S. Poncin, G. Wild, N. Midoux, *Chem. Eng. Proc.* **2001**, *40*, 135.

[6] J. P. Giovannettone, E. Tsai, J. S. Gulliver, *Chem. Eng. J.* **2009**, *149*, 301. DOI: 10.1016/j.cej.2008.11.024

[7] W.-D. Deckwer, *Bubble Column Reactors*, John Wiley & Sons, Chichester **1992**.

[8] A. I. Shnip, R. V. Kolhatkar, D. Swamy, J. B. Joshi, *Int. J. Multiphase Flow* **1992**, *18*, 705.

[9] M. C. Ruzicka, N. H. Thomas, *Int. J. Multiphase Flow* **1997**, *29*, 249.

[10] B. N. Thorat, J. B. Joshi, *Exp. Therm. Fluid Sci.* **2004**, *28*, 423.

[11] C. P. Ribeiro, Jr., *Chem. Eng. J.* **2008**, *140*, 473. DOI: 10.1016/j.cej.2007.11.029

[12] B. G. Kelkar, *Chem. Eng. Commun.* **1986**, *41*, 237.

[13] P. M. Wilkinson, A. P. Spek, L. L. van Dierendonck, *AIChE J.* **1992**, *38*, 544.

[14] A. Sarrafi, M. Jamialahmadi, H. Müller-Steinhagen, J. M. Smith, *Can. J. Chem. Eng.* **1999**, *77*, 11.

[15] A. Shaikh, M. H. Al-Dahhan, *Int. J. Chem. React. Eng.* **2007**, *5*, 1.

[16] D. J. McCann, R. G. H. Prince, *Chem. Eng. Sci.* **1971**, *26*, 1505.

[17] M. C. Ruzicka, J. Drahos, M. Fialova, N. H. Thomas, *Chem. Eng. Sci.* **2001**, *56*, 6117.

[18] S. Nedeltchev, A. Shaikh, M. Al-Dahhan, *Chem. Eng. Technol.* **2006**, *29*, 1054. DOI: 10.1002/ceat.200600162

[19] S. Nedeltchev, U. Jordan, O. Lorenz, A. Schumpe, *Chem. Eng. Technol.* **2007**, *30*, 534. DOI: 10.1002/ceat.200600344

[20] E. Olmos, C. Gentric, S. Poncin, N. Midoux, *Chem. Eng. Sci.* **2003**, *58*, 1731. DOI: 10.1016/S0009-2509 (03)00002-2

[21] E. Olmos, C. Gentric, N. Midoux, *Can. J. Chem. Eng.* **2003**, *81*, 382.

[22] S. Barghi, A. Prakash, A. Margaritis, M. A. Mergougnou, *Can. J. Chem. Eng.* **2004**, *82*, 865.

[23] R. C. Chen, J. Reese, L.-S. Fan, *AIChE J.* **1994**, *40*, 1093.

[24] T.-J. Lin, J. Reese, T. Hong, L.-S. Fan, *AIChE J.* **1996**, *42*, 301.

[25] P. Grasberger, I. Procaccia, *Phys. Rev. A* **1983**, *28*, 2591.

[26] J. C. Schouten, F. Takens, C. M. Van den Bleek, *Phys. Rev. E* **1994**, *49*, 126.

[27] C. M. Van den Bleek, J. C. Schouten, *Chem. Eng. J.* **1993**, *53*, 75.

[28] H. M. Letzel, J. C. Schouten, R. Krishna, C. M. van den Bleek, *Chem. Eng. Sci.* **1997**, *52*, 4447.

[29] A. Shaikh, *D.Sc. Thesis*, Washington University, St. Louis **2007**.

[30] A. Shaikh, M. Al-Dahhan, *AIChE J.* **2009**, submitted.

[31] M. Jamialahmadi, H. Müller-Steinhagen, *Dev. Chem. Eng.* **1992**, *1*, 16.

[32] T.-J. Lin, R.-C. Juang, Y.-C. Chen, C.-C. Chen, *Chem. Eng. Sci.* **2001**, *56*, 1057.

[33] R. Krishna, J. Ellenberger, C. Maretto, *Int. Commun. Heat Mass Transfer* **1999**, *26*, 467.

[34] R. Clift, J. R. Grace, M. E. Weber, *Bubbles, Drops and Particles*, 1st ed., Academic Press, New York **1978**.

[35] L.-S. Fan, K. Tsuchiya, *Bubble Wake Dynamics in Liquids and Liquid-Solid Suspensions*, 1st ed., Butterworth-Heinemann, Stoneham, MA **1990**.

[36] K. Terasaka, Y. Inoue, M. Kakizaki, M. Niwa, *J. Chem. Eng. Jpn.* **2004**, *37*, 921.

[37] J. Ellenberger, R. Krishna, *Chem. Eng. Sci.* **1994**, *49*, 5391.

[38] S. Nedeltchev, *Bulg. Chem. Ind.* **1998**, *69*, 35.

 © 2011 WILEY-VCH Verlag GmbH & Co. KGaA, Weinheim

15214125, 2011, 2, Downloaded from https://onlinelibrary.wiley.com/doi/10.1002/ceat.201000308 by Missouri University Of Science, Wiley Online Library on [10/04/2023]. See the Terms and Conditions (https://onlinelibrary.wiley.com/terms-and-conditions) on Wiley Online Library for rules of use; OA articles are governed by the applicable Creative Commons License

[39] R. C. Darton, R. D. LaNauze, J. F. Davidson, D. Harrison, *Trans. Inst. Chem. Eng.* **1977**, *55*, 274.
[40] R. Krishna, J. Ellenberger, D. E. Hennephof, *Chem. Eng. J.* **1993**, *53*, 89.
[41] S. Nedeltchev, S. Ookawara, K. Ogawa, *J. Chem. Eng. Jpn.* **1999**, *32*, 431.
[42] S. Nedeltchev, S. Ookawara, K. Ogawa, *J. Chem. Eng. Jpn.* **2000**, *33*, 761.
[43] S. Nedeltchev, S. B. Kumar, M. C. Dudukovic, *Can. J. Chem. Eng.* **2003**, *81*, 367.
[44] S. Nedeltchev, S. Ookawara, K. Ogawa, *Can. J. Chem. Eng.* **2003**, *81*, 597.
[45] D. N. Miller, *AIChE J.* **1974**, *20*, 445.

 © 2011 WILEY-VCH Verlag GmbH & Co. KGaA, Weinheim

15214125, 2011, 2, Downloaded from https://onlinelibrary.wiley.com/doi/10.1002/ceat.201000308 by Missouri University Of Science, Wiley Online Library on [10/04/2023]. See the Terms and Conditions (https://onlinelibrary.wiley.com/terms-and-conditions) on Wiley Online Library for rules of use; OA articles are governed by the applicable Creative Commons License